

HAMAMATSU PRESENTS

ANALYTICAL TALKS

WATCH NOW 



Flash Scanning Volumetric Optoacoustic Tomography for High Resolution Whole-Body Tracking of Nanoagent Kinetics and Biodistribution

Avihai Ron, Sandeep Kumar Kalva, Vijitha Periyasamy, Xosé Luís Deán-Ben, and Daniel Razansky*

Tracking of biodynamics across entire living organisms is essential for understanding complex biology and disease progression. The presently available small-animal functional and molecular imaging modalities remain constrained by factors including long image acquisition times, low spatial resolution, limited penetration or poor contrast. Here flash scanning volumetric optoacoustic tomography (fSVOT), a new approach for high-speed imaging of fast kinetics and biodistribution of optical contrast agents in whole mice that simultaneously provides reference images of vascular and organ anatomy with unrivaled fidelity and contrast, is presented. The imaging protocol employs continuous overfly scanning of a spherical matrix array transducer, accomplishing a 200 μm resolution 3D scan of the whole mouse body within 45 s without relying on signal averaging. This corresponds to an imaging speed gain of more than an order of magnitude compared with existing state-of-the-art implementations of comparable resolution performance. Volumetric tracking and quantification of gold nanoagent and near infrared (NIR)-II dye kinetics and their differential uptake in various organs are demonstrated. fSVOT thus offers unprecedented capabilities for multiscale imaging of pharmacokinetics and biodistribution with high contrast, resolution, and speed.

1. Introduction

Preclinical imaging plays an indispensable role in studies of disease pathophysiology and monitoring of treatments. Broad availability of transgenic, knock-out/in mouse models have fostered the adaptation of clinical imaging modalities for small animal imaging applications, including computed tomography (CT), positron emission tomography (PET), single-photon emission computed tomography, and magnetic resonance imaging (MRI).^[1] New types of techniques were further developed to provide superior functional and molecular optical contrast relying on fluorescence or optoacoustic (OA) excitation.^[2] High spatiotemporal resolution is of particular importance for the characterization of toxicity, biodistribution, and metabolic clearance of drugs and contrast agents.^[3] To this end, pharmacokinetic studies assisted with targeted contrast agents have greatly facilitated the evaluation of new therapies, accelerated drug discovery,

and enabled optimizing the administration routes for effective treatment of diseases.^[4]


In the cancer research field, gold nanoparticles (AuNP) have shown to offer promising theranostic properties,^[5,6] yet safety concerns related to accumulation and elimination from the body call for a better understanding of their pharmacokinetics and biocompatibility.^[7] Studies involving large numbers of animals are commonly required to assess toxicity of nanoparticles and other exogenously administered agents, turning imaging throughput into a key factor for determining their efficiency.^[8] Acceleration of the scanning time is further essential for properly assessing the dynamic biodistribution of the administered agents. However, total-body scan times of most small animal molecular imaging modalities remain in the 10–20 min range,^[9] restricting their applicability for efficient visualization of biological dynamics at the whole body level.

Optoacoustic tomography (OAT) has recently matured into a highly versatile molecular imaging technology for preclinical research.^[10] It capitalizes on rich optical contrast combined with fast and high-resolution ultrasound-based image formation

A. Ron, V. Periyasamy, Prof. D. Razansky
Institute for Biological and Medical Imaging
Technical University of Munich and Helmholtz Center
Munich D-85764, Germany
E-mail: daniel.razansky@uzh.ch

Dr. S. K. Kalva, Dr. X. L. Deán-Ben, Prof. D. Razansky
Institute of Pharmacology and Toxicology and Institute for Biomedical
Engineering, University of Zurich
Zurich CH-8057, Switzerland

Dr. S. K. Kalva, Dr. X. L. Deán-Ben, Prof. D. Razansky
Institute for Biomedical Engineering
Department of Information Technology and Electrical Engineering
ETH Zurich CH-8093, Switzerland

 The ORCID identification number(s) for the author(s) of this article can be found under <https://doi.org/10.1002/lpor.202000484>

© 2021 The Authors. Laser & Photonics Reviews published by Wiley-VCH GmbH. This is an open access article under the terms of the Creative Commons Attribution-NonCommercial License, which permits use, distribution and reproduction in any medium, provided the original work is properly cited and is not used for commercial purposes.

DOI: 10.1002/lpor.202000484

to resolve a myriad of endogenous and exogenous substances featuring distinctive light absorption profiles.^[11] Small-animal OAT scanners based on different acquisition geometries are increasingly exploited in various biological applications.^[12,13] Whole-body tomographic imaging of mice is typically achieved via scanning of ultrasound arrays with the imaging speed and image quality mainly determined by the array configuration and scanning geometry. For example, concave arrays of cylindrically focused transducers provide cross-sectional (2D) views in real time, but lack the angular coverage required for accurate volumetric (3D) imaging.^[14–16] Ideally, a large number of pressure signals should be acquired around the imaged object in order to achieve accurate reconstruction of arbitrarily oriented vascular structures.^[17,18] Recently, spiral volumetric optoacoustic tomography (SVOT) achieved unprecedented image quality by capitalizing on the large angular coverage of a custom-made spherical array.^[19] SVOT further enabled scaling the effective temporal resolution to the desired field of view (FOV), greatly improving the throughput capacity for studying biological dynamics and biodistribution of agents. Yet, high speed imaging was restricted to small (single organ) regions,^[20] hampering the visualization of fast kinetics on a larger scale. Generally, at least 10–20 min are required for acquiring high resolution full body scans with state-of-the-art OAT systems, which prevents leveraging the full advantage of the superior resolution and molecular sensitivity of OAT for visualizing large scale biodynamics.

Herein, we introduce flash scanning volumetric optoacoustic tomography (fSVOT), a new approach for high-speed imaging of fast kinetics and biodistribution of optical contrast agents in the second near infrared (NIR-II) window in entire mice. The method effectively reduces high-resolution total-body image acquisition times to sub-minute levels, thus taking whole-body small animal molecular imaging to a new level of spatiotemporal resolution performance.

2. Results and Discussion

2.1. The fSVOT

A detailed description of the fSVOT experimental system design is provided as Figures S1 and S2 in the Supporting Information. Briefly, the concept of fSVOT relies on continuous overfly scanning of a spherical matrix array transducer assisted with micrometer-scale precision readings from laser distance sensors. The system captures individual volumetric OA images covering $\sim 1 \text{ cm}^3$ field-of-view after every pulsed laser excitation (Figure 1a). Following full translation and rotation cycles, the individual volumes at each scan position are combined together to arrive at the whole-body mouse image. In this way, a 3D total-body scan with $\sim 200 \mu\text{m}$ spatial resolution is accomplished within 45 s without relying on signal averaging (see the Experimental Section for details). To investigate the effect of scanning velocity on the resolution and contrast of the images rendered by the system, a phantom incorporating thin sutures was scanned at velocities spanning 20–80 mm s^{-1} range (Figure 1b). The contrast-to-noise ratio (CNR) of the images was estimated as the ratio between image contrast (i.e., difference between peak signal and background) and noise calculated as standard deviation of the background. As expected, the CNR of individual frames

corresponding to single-shot emission of the laser is similar and independent of the scanning velocity (Figure 1c). When superimposing multiple frames to render a larger FOV, the contrast worsens when increasing imaging speed (Figure 1d). This is consistent with the fact that the scanning speed dictates the effective number of overlapping frames used for rendering the superimposed image, and hence the effective number of averaged voxels. As the CNR is expected to be proportional to the square root of the number of superimposed frames—inversely proportional to the scanning velocity—dividing the CNR values of the image by the inverse of the square root of the corresponding scanning velocity renders comparable normalized values (Figure 1e). Further analysis of the horizontal and vertical amplitude profiles (Figure 1f) confirms that the spatial resolution, i.e., full width at half maximum (FWHM) of the line profiles, remains unaltered irrespective of the scanning velocity.

2.2. Whole-Body fSVOT

Figure 1g shows a sequence volumetric OAT frames acquired from a mouse scanned at 40 mm s^{-1} velocity and 1064 nm excitation wavelength, yielding a separation of 0.4 mm between consecutive frames. Owing to the large FOV of the detector, neighboring frames share overlapping regions and anatomical structures (Figure 1h). By adding up frames acquired by a single vertical sweep, a large FOV spanning 4.5 cm length can be readily acquired within just 1 s (Figure 1i), where the effect of CNR enhancement via spatial integration of multiple volumetric frames is clearly visible. By following a zigzag trajectory (Figure 1a), fSVOT is then capable of full-body imaging in less than 1 min.

The maximum intensity projections (MIPs) of the 3D whole-body mouse images acquired within 45 s are shown in Figure 2, offering detailed anatomical information of the thorax and abdominal regions. Main organs like the kidney or the spleen as well as the spine and the surrounding vascular system are clearly discernible with high resolution and contrast. Finer structures such as thoracic and femoral vessels can also be observed. Notably, the full 360° angular coverage of the system facilitates visualization of deep anatomical structures, which are concealed by the projection (MIP) views that commonly emphasize superficial signals. This is further evident in the cross-sectional slice images (Figure S3, Supporting Information). Note that majority of the intrinsic vascular contrast at the 1064 nm illumination wavelength is contributed by absorption of the water and oxygenated hemoglobin molecules (Figure 3a). The spectrum of individual substance in Figure 3a was normalized with respective peak maximum value within the spectral range of 700–1250 nm. A video showing rotational 3D views of the reconstructed data is further available in Video S1 in the Supporting Information.

2.3. In Vivo Biodistribution of Gold Nanoagent and NIR-II Dye

We subsequently exploited the unique spatiotemporal resolution properties of fSVOT to track fast kinetics and biodistribution of AuNP having peak absorption around 1070 nm (Figure 3a) at the whole-body scale. Generally, substances can be cleared from the blood circulation either by being filtered in the kidneys or metabolized in the liver. Also, some nanoparticles are known to accumulate in the spleen. The kinetics are affected by the shape as

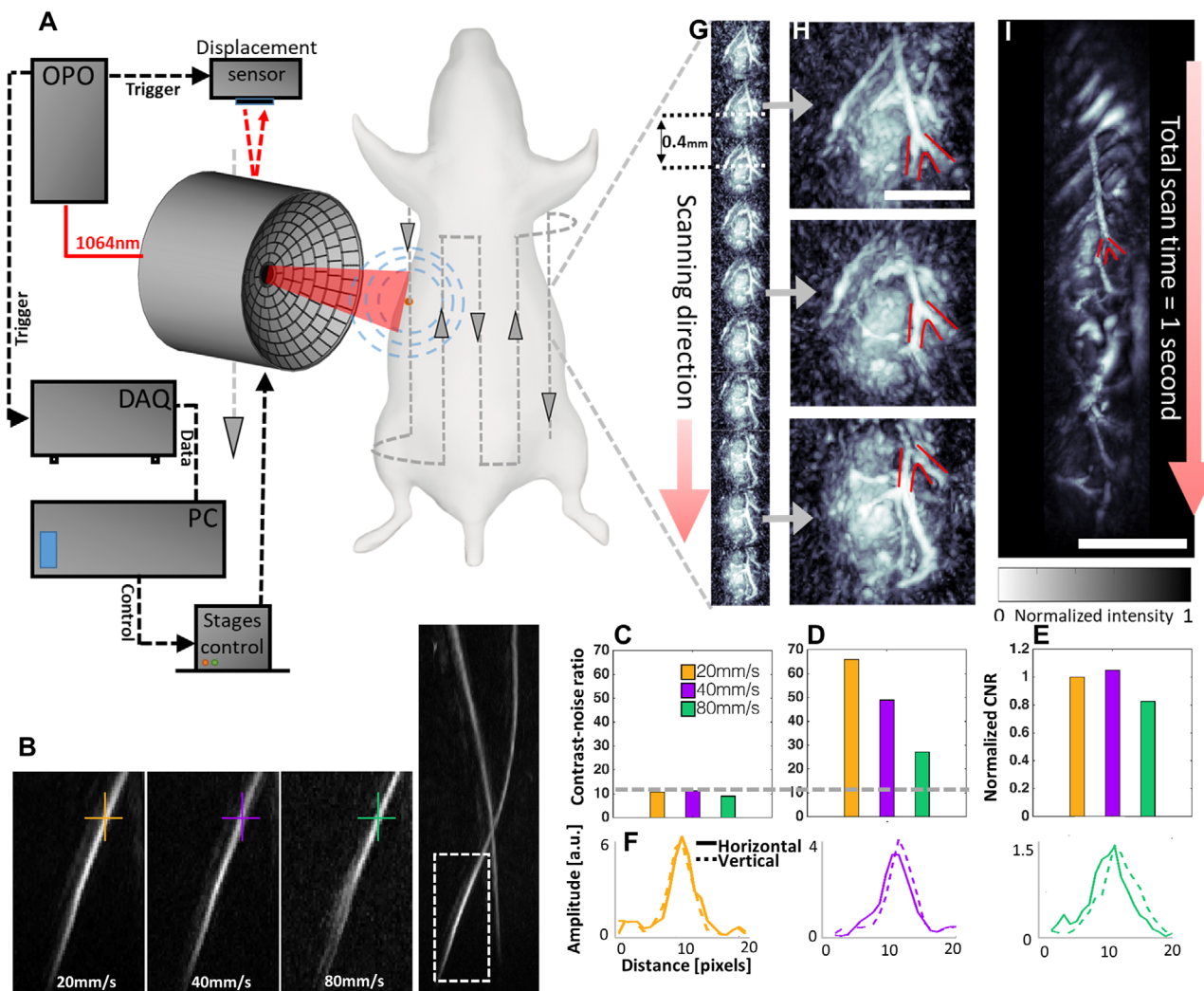


Figure 1. The flash scanning volumetric optoacoustic tomography (fSVOT) approach. A) Schematics of the imaging system. The spherical matrix ultrasonic transducer array is translated and rotated 360° around the animal in an overfly scanning mode. Light is transmitted through an aperture in the center of the array. Data acquisition is triggered by the optical parametric oscillator (OPO) laser source and synchronized with a displacement sensor, which continuously samples the detector position. B) Maximal intensity projection (MIP) of the 3D rendering of a phantom containing two sutures. The effect of the different scanning velocities on the image contrast is shown in the three zoom-ins. C) Contrast-to-noise ratio (CNR) values of an individual volumetric image frame of the phantom at the three scanning velocities. D) CNR analysis of a larger compounded volume of a phantom. E) CNR values after normalizing by the square root of scanning velocity. F) 1D OA signal profiles along the vertical and horizontal directions, as marked in (B). G) Consecutive OA image volumes acquired from a mouse at a vertical scanning velocity of 40 mm s⁻¹, corresponding to 0.4 mm separation between the consecutive frames. H) Zoom-ins on three representative frames from panel (G) sharing the same anatomical structure (marked in red). I) Rendering of a larger FOV acquired by a 1 s vertical sweep of the scanner. The same anatomical structure from (H) is also visible (marked in red). Scale bar—1 cm.

well as other properties of nanoagents. Accumulation level and kinetics of excretion in the selected organs are then of particular interest as they are directly linked to the potential toxicity of the injected agents. Specifically, the analysis of AuNP was concentrated in the spleen and liver areas, regarded as the two main sites of AuNP accumulation *in vivo*. fSVOT scanning at 40 mm s⁻¹ allowed for full 360° coverage between the thorax and abdominal regions within ~45 s scanning time. In this way, longitudinal responses in multiple anatomical locations could be simultaneously tracked with high spatial and temporal resolution. Gold nanorod (AuNR) agent accumulation in the spleen and liver are illustrated in Figure 3b,c, exhibiting a gradual increase in the

local signal amplitudes. The high OA image contrast in these regions was further exploited to perform volumetric segmentations, which enabled accurate signal quantification over entire organs (Figure 3d). Whilst the liver accumulation leveled off at 19% above the baseline signal at 1 min after the AuNP administration, the spleen signal plateaued at 27% above the baseline, 2 min post injection (Figure 3e). As expected, no agent perfusion through the kidneys has been observed. Generally, an initial signal increase is expected as the agent circulates throughout the whole vasculature of the animal body. This is followed by an AuNR signal decrease in the kidneys as the agent clears from the blood. The AuNR signal changes in the liver and spleen are in fact

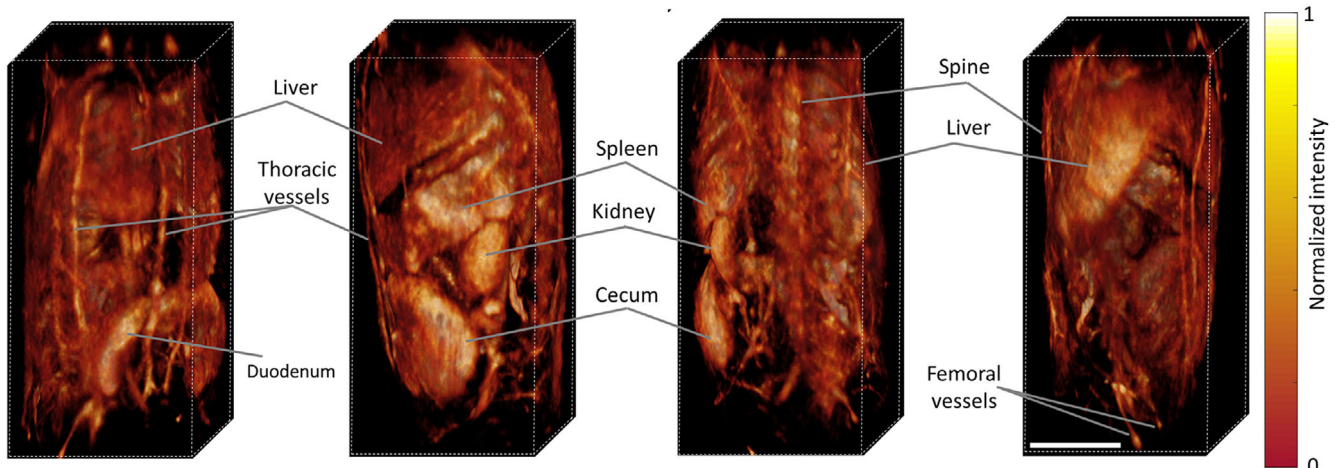


Figure 2. Rapid whole-body 3D images acquired noninvasively with flash scanning volumetric optoacoustic tomography (fSVOT) using 40 mm s^{-1} scanning velocity (45 s total scan time). Maximal intensity projections (MIPs) of the rendered volume are shown from the front, left, back, and right views. Selected anatomical structures are labeled. Scale bar—1 cm.

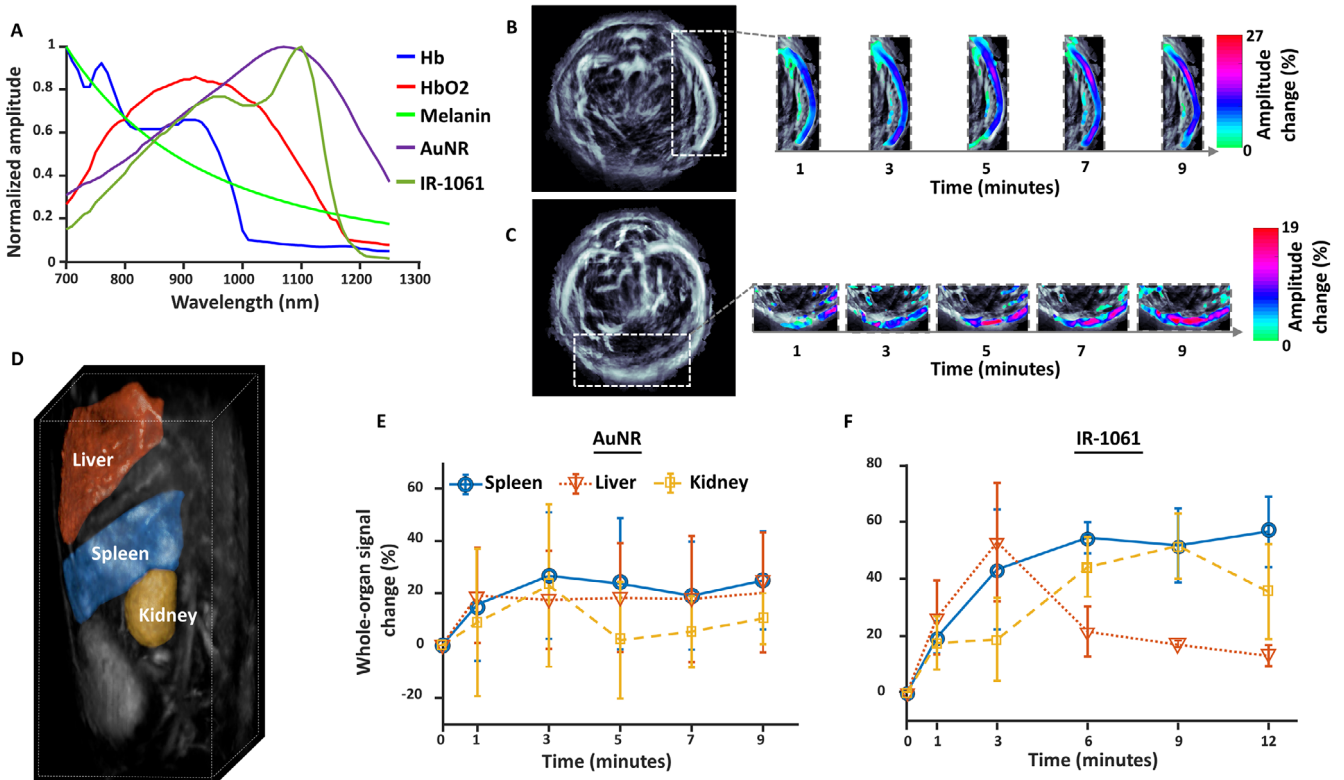


Figure 3. Rapid high-resolution 3D tracking of nanoagent kinetics in whole mice with flash scanning volumetric optoacoustic tomography (fSVOT). A) Optical extinction spectra of main tissue chromophores along with the AuNP and IR-1061 spectra. B) Cross-sectional images showing OA signal increase due to AuNP accumulation in the spleen. The zoom-ins display the OA signal amplitude changes in a single slice over time (superimposed in color) in response to AuNP administration. C) The corresponding slice images showing AuNP accumulation in the liver. D) 3D location of the segmented organ volumes used for quantitative biodistribution analyses (liver—red, spleen—blue, and kidney—yellow). E) Volumetric OA signal changes (baseline subtracted) measured across the whole liver, spleen, and kidney regions, following injection of AuNR ($n = 5$ mice). F) The corresponding signal changes after the IR-1061 dye injection ($n = 3$ mice).

insignificant after 3 min and may lie within measurement uncertainties. Same is true for the slight signal increase in the kidneys at 9 min. Note that the Y-axis represents the relative signal change with respect to the signal at 0 timepoint. A negative signal decrease might have been caused by a number of measurement imperfections not directly related to the probe concentration, such as slight motion of the mouse during the injections, laser energy instabilities, and light intensity variations inside the mouse due to an increased tissue absorption by the contrast agent. Such negative values are more prominent when the signal variations are small and may be amplified by normalizing to a low background in some regions. Yet, consistent signal trends were observed when averaging across several measurements. Note that the error bar was calculated as the standard deviation of the relative signal change (in percentage) of all the five mice at respective individual time points. The control experiments using phosphate buffered saline (PBS) injections ($n = 3$ mice) further confirmed negative to no-response in both liver and spleen (Figure S4, Supporting Information).

To further illustrate the capabilities of fSVOT for differentiating the organ kinetics, we injected an aqueous solution of IR-1601 dye with peak absorption in the NIR-II region (Figure 3a). In principle, due to the small size of the IR-1601 molecules, preferential kidney clearance is expected in this case.^[21] However, the dye is only partially soluble in water,^[22] which was confirmed by our dynamic light scattering (DLS) measurements of the solution, revealing the presence of particles with an average diameter of 600 nm (Figure S5, Supporting Information), arguably corresponding to larger aggregation of the IR-1061 molecules. As a result, the clearance mechanism differed from AuNR in this case, namely, the IR-1061 dye strongly accumulated in the kidney and spleen regions with the signal peaking at 51% and 54% above the baseline levels, respectively (Figure 3f).

3. Conclusions

We report on a fSVOT technique for rapid anatomical and functional imaging of small animals. Whole body panoramic (360°) imaging of mice was achieved with 200 μm resolution in 45 s scan time with the new technique, which employs a continuous overfly scanning of the spherical array probe assisted with high micrometer-scale precision readings from laser distance sensors. This corresponds to more than an order of magnitude acceleration of the whole-body image acquisition speed compared to previously reported systems employing a point-by-point (stop and go) scanning method,^[19] which further necessitated animal repositioning for a full body 360° scan. This step change in performance has enabled imaging of fast kinetics and biodistribution of optical contrast agents not possible with the previously reported approaches. The whole body imaging speed of fSVOT is comparable to state-of-the-art anatomical micro-CT scanners^[23] and greatly outperforms scan times of other tomographic imaging techniques such as MRI or PET.^[24] Furthermore, when the spherical matrix array is kept at a stationary position, the system can be used for real-time visualization of agent perfusion dynamics in blood vessels^[25] and at the whole organ scale at unmatched volumetric frame rates in the kilohertz range,^[26] thus providing unique scalability across different spatial and temporal dimensions not achievable with other imaging

modalities. System characterization suggests that image contrast of the compounded volumes is exclusively dependent upon scanning velocity, which enables scaling the imaging speed to the desired image quality. Note that respiratory motion suppression algorithms^[27] and gated acquisition approaches^[28,29] may further be employed to enhance image quality.

fSVOT achieved dynamic monitoring of agents in 3D at the whole-body scale while simultaneously tracking early accumulation and clearance of AuNP and IR-1601 dye across different organs. AuNP are known to allow for multiplexed targeting, diagnostic, and therapeutic functionalities^[30] and are particularly suited for OAT due to their strong and tunable absorption properties. Tuning the AuNP shape to absorb light at 1064 nm facilitates deep tissue imaging due to the reduced light attenuation and scattering by living tissues and the availability of high energy short pulsed lasers emitting at this wavelength. Furthermore, due to the lower absorption of HbO₂ and the overall diminished background tissue contrast in the NIR-II spectral window (>1000 nm),^[31] new contrast agents are constantly developed to capitalize on their deep tissue imaging advantages.^[32] In previous works, OA tracking of nanoagents in mice has been accomplished with typical total-body scanning times of several hours,^[33] or, alternatively, by confining detection to a single cross-section.^[34,35] Owing to its fast scanning times, differences in settling times between the different organs could readily be discerned with fSVOT, in agreement with previous reports that employed cross-sectional imaging systems. At present, only micro-CT was shown to render similar throughput, yet it provides significantly lower sensitivity to AuNP and other extrinsic agents^[36] and is further afflicted by the use of ionizing radiation. fSVOT can potentially be further accelerated to achieve faster frame rates, e.g., by using arrays with more elements or other scanning trajectories. Here several challenges are anticipated, such as vibrations, instabilities, or bubble formation during fast scans or potential tissue damage when operating at higher laser pulse repetition rates.

The capacity for fast tracking of agent kinetics is of particular importance in cancer research, e.g., to assess vascular perfusion function or study accumulation and retention of nanodrug formulations in tumors.^[37] Whole-body imaging on sub-minute time scales with superb contrast and resolution offers new venues for studying pharmacokinetics and pharmacodynamics of nanoparticulate agents, their accumulation, and clearance mechanisms in health and disease. fSVOT further offers a broad selection of contrast molecules and nanoparticles not detectable with other well-established modalities such as PET or MRI. This is because any substance with distinct optical absorption characteristics may serve for optoacoustic contrast enhancement. In addition to its superior functional and molecular imaging capabilities, fSVOT renders excellent anatomical reference images mainly stemming from its strong intrinsic vascular and hemoglobin-related contrast. The true volumetric nature of fSVOT has the potential to further refine quantitative readings as compared to the commonly employed cross-sectional OA imaging approaches.^[38] Note that continuous exposure of AuNP to nanosecond pulsed laser illumination has been reported to lead to significant OA signal degradation,^[39] primarily attributed to their poor thermal stability. This may hamper quantification of time-lapse dynamics and biodistribution.^[40] Yet, constant

motion of the detection array and light illumination elements in our implementation helps mitigating AuNP photodegradation by reducing light exposure to a single laser pulse or a small number of pulses.

In summary, we demonstrated the feasibility of rapid high-resolution 3D OA tracking of nanoparticle kinetics in whole mice. The newly introduced continuous scanning scheme boosts the throughput capacity of OAT while enabling time-lapse multiplexed observations into early agent accumulation across multiple organs. All in all, fSVOT offers unprecedented abilities for preclinical whole-body anatomical, functional and molecular imaging of pharmacokinetics and biodistribution with high contrast, resolution, and speed.

4. Experimental Section

Experimental Setup: The layout of the experimental system is depicted in Figure 1a. The spherical matrix transducer array (Imasonic SaS, Voray, France) is mounted on motorized stages (International Automation Industry Inc., Japan) that are continuously rotated and vertically translated around the sample. The vertical motor provides load capacity of up to 8 kg and can cover a range of up to 15 cm, reaching a scanning velocity of 80 mm s^{-1} . The rotation motor was programmed to complete a full 360° rotation in 15° steps. The sample was placed in a custom-made holder and immersed in a water tank to facilitate efficient propagation and detection of the optoacoustically generated pressure waves. OA signals were generated with a short-pulsed ($<10 \text{ ns}$) laser source (SpitLight, Innolas Laser GmbH, Germany) operating at 1064 nm . The pulse repetition frequency of the laser was set to 100 Hz . Light was guided via a custom-made fiber bundle through a central aperture of the array, thus creating a Gaussian illumination profile with a size of $\sim 10 \text{ mm}$ at the FWHM. The per-pulse energy at the fiber output was kept below 15 mJ . The array consists of 256 elements (element area of 9 mm^2) arranged on a hemispherical surface with a radius of 4 cm and 90° angular coverage.^[41] The elements have central frequency of 4 MHz and -6 dB bandwidth of $\sim 100\%$, resulting in nearly isotropic imaging resolution in the $200 \text{ }\mu\text{m}$ range.^[19] The recorded time-resolved OA signals were digitized at $40 \text{ megasamples s}^{-1}$ by a custom-made data acquisition system (DAQ; Falkenstein Mikrosysteme GmbH, Germany). The precise vertical position of the array was sampled by a sensitive ($16 \text{ }\mu\text{m}$ resolution, sampling cycle-up to $3 \text{ }\mu\text{s}$) laser displacement sensor (Keyence GmbH, Germany). The DAQ and displacement sensor were simultaneously triggered by the Q-switch output of the laser. The data recorded by all the 256 channels were transmitted to the personal computer (PC) via 1 Gb Ethernet connection for further processing. Data acquisition and motor positioning were computer-controlled using MATLAB (Mathworks, MA, USA).

System Characterization: Calibration of the relative position and orientation of the array with respect to the rotation axis was performed by scanning at multiple angular locations around a single $100 \text{ }\mu\text{m}$ polyethylene microsphere (Cospheric Inc, Santa Barbara, USA) embedded in an agar phantom. The exact time delay between the signal acquisition and readings of the laser displacement sensor was calibrated by vertically scanning the same microsphere phantom. To further examine the effect of different scanning velocities on the image quality, an agar phantom containing two black $125 \text{ }\mu\text{m}$ diameter surgical sutures (Ethicon, USA) forming a cross-shape was molded. The phantom was scanned in continuous motion at velocities of $20, 40, \text{ and } 80 \text{ mm s}^{-1}$. CNR analysis was performed on individual frames as well as the fully rendered images. Next, vertical and horizontal amplitude profiles along the suture were compared. Data analysis was executed in MATLAB.

Whole-Body and Biodistribution Imaging: All animal in vivo experiments were performed in full compliance with the institutional guidelines of the Helmholtz Center Munich and approved by the government of Upper Bavaria. Hairless immunodeficient mice (Envigo, Germany) were

anesthetized (2% isoflurane v/v) and placed in a custom-made holder, which was used to maintain the mice in a stationary position along the center of rotational scanning. The fore and hind paws were attached to the holder during the experiment. The mice were then immersed inside the water tank with their head remaining outside the water. The temperature of the water tank was maintained at 34°C with a feedback-controlled heating stick. A breathing mask with a mouth clamp was used to fix the head in an upright position and supply anesthesia and oxygen. Injections ($n = 5$ mice) of $150 \text{ }\mu\text{L}$ gold nanorods ($10 \times 67 \text{ nm}$, surface plasmon resonance (SPR) wavelength = 1064 nm , 2.5 mg mL^{-1} PBS, Nanopartz Inc., USA) as well as $150 \text{ }\mu\text{L}$ of clean PBS for control experiments were done intravenously via a tail-catheter ($n = 3$ mice), while the animals were positioned inside the imaging setup. Similarly, different kinetics of IR-1061 dye using the fSVOT system were observed after injecting $150 \text{ }\mu\text{L}$: solution of the dye diluted in PBS at a concentration of 0.52 mg mL^{-1} and filtered with a $5 \text{ }\mu\text{m}$ pore size (PluriStrainer 5, pluriSelect Life Science, Leipzig, Germany) through the tail-vein ($n = 3$ mice).

Image Reconstruction and Analysis: The time-resolved signals from the 256 detection elements of the array were band-pass filtered (between 0.25 and 6 MHz) and deconvolved with the impulse response of the array elements. The filtered signals were used to reconstruct volumetric images covering $\sim 1 \text{ cm}^3$ FOV for each laser pulse using graphics processing unit (GPU) implementation of a 3D back-projection algorithm.^[42] A designated reconstruction approach (see the Supporting Information for more details) consisted in spatial compounding of the volumes acquired in the overfly mode based on accurately synchronized laser distance sensors readings, which greatly contributed to CNR enhancement. This was particularly done by mapping the transducer elements' coordinates onto volumetric image grid ($100 \text{ }\mu\text{m}$ pixel resolution) using known positions of the stages retrieved from the displacement sensor's readings. 3D visualization of the OA images was done with Amira (Visual Sciences Group).

The image intensity values were further normalized in the individual reconstructed volumes with an exponential decay function to compensate for light attenuation with depth hence facilitating quantification of agent kinetics and biodistribution across different organs. To quantify the changes in biodistribution of contrast agents across different organs, a volumetric mask of each organ was manually delineated. Next, the OA signal amplitude within each organ was quantified. Finally, the ratios between the baseline signal (prior to injection) and the signals at different time points following the injection were calculated. Analyses were carried out using MATLAB.

Supporting Information

Supporting Information is available from the Wiley Online Library or from the author.

Acknowledgements

The authors wish to thank M. Reiss for his support with the measurements and animals handling, L. Reith for his support with the DLS measurements, S. Glasl, P. Anzenhofer, and U. Klemm for their valuable advice. This project has received funding from the European Research Council Consolidator Grant ERC-2015-CoG-682379.

Open access funding enabled and organized by Projekt DEAL.

Conflict of Interest

The authors declare no conflict of interests.

Data Availability Statement

Research data are not shared.

Keywords

continuous scanning, gold nanorods, optoacoustic imaging, pharmacokinetics, photoacoustic tomography, photodamage, photodegradation, second near-infrared window

Received: November 1, 2020

Revised: December 26, 2020

Published online: February 15, 2021

- [1] M. Baker, *Nature* **2010**, 463, 977.
- [2] R. Weissleder, M. Nahrendorf, *Proc. Natl. Acad. Sci. U. S. A.* **2015**, 112, 14424.
- [3] K. O. Vasquez, C. Casavant, J. D. Peterson, *PLoS One* **2011**, 6, e20594.
- [4] J. R. Conway, N. O. Carragher, P. Timpson, *Nat. Rev. Cancer* **2014**, 14, 314.
- [5] A. R. Rastinehad, H. Anastos, E. Wajswol, J. S. Winoker, J. P. Sfakianos, S. K. Doppalapudi, M. R. Carrick, C. J. Knauer, B. Taouli, S. C. Lewis, *Proc. Natl. Acad. Sci. U. S. A.* **2019**, 116, 18590.
- [6] N. S. Abadeer, C. J. Murphy, *J. Phys. Chem. C* **2016**, 120, 4691.
- [7] N. Khlebtsov, N. Dykman, *Chem. Soc. Rev.* **2011**, 40, 1647.
- [8] N. Aide, C. Desmonts, M. Briand, M. Meryet-Figuere, L. Poulain, *Nucl. Med. Commun.* **2010**, 31, 851.
- [9] G. C. Kagadis, N. L. Ford, D. N. Karnabatidis, G. K. Loudos, *Handbook of Small Animal Imaging: Preclinical Imaging, Therapy, and Applications*, CRC Press, Boca Raton, FL **2016**.
- [10] X. Deán-Ben, S. Gottschalk, B. Mc Larney, S. Shoham, D. Razansky, *Chem. Soc. Rev.* **2017**, 46, 2158.
- [11] J. Weber, P. C. Beard, S. E. Bohndiek, *Nat. Methods* **2016**, 13, 639.
- [12] J. Reber, M. Willershäuser, A. Karlas, K. Paul-Yuan, G. Diot, D. Franz, T. Fromme, S. V. Ovsepian, N. Bézière, E. Dubikovskaya, D. C. Karampinos, C. Holzapfel, H. Hauner, M. Klingenspor, V. Ntziachristos, *Cell Metab.* **2018**, 27, 689.
- [13] K. Basak, X. Luís Deán-Ben, S. Gottschalk, M. Reiss, D. Razansky, *Light: Sci. Appl.* **2019**, 8, 71.
- [14] V. Ntziachristos, D. Razansky, *Chem. Rev.* **2010**, 110, 2783.
- [15] E. Merčep, J. L. Herraiz, X. L. Deán-Ben, D. Razansky, *Light: Sci. Appl.* **2019**, 8, 18.
- [16] L. Li, L. Zhu, C. Ma, L. Lin, J. Yao, L. Wang, K. Maslov, R. Zhang, W. Chen, J. Shi, L. V. Wang, *Nat. Biomed. Eng.* **2017**, 1, 0071.
- [17] D. Van de Sompel, L. S. Sasportas, J. V. Jokerst, S. S. Gambhir, *PLoS One* **2016**, 11, e0152597.
- [18] S. Ermilov, R. Su, A. Conjusteau, F. Anis, V. Nadvoretzkiy, M. Anastasio, A. Oraevsky, *Ultrason. Imaging* **2016**, 38, 77.
- [19] T. F. Fehm, X. L. Deán-Ben, S. J. Ford, D. Razansky, *Optica* **2016**, 3, 1153.
- [20] X. L. Deán-Ben, T. F. Fehm, S. J. Ford, S. Gottschalk, D. Razansky, *Light: Sci. Appl.* **2017**, 6, e16247.
- [21] Z. Tao, G. Hong, C. Shinji, C. Chen, S. Diao, A. L. Antaris, B. Zhang, Y. Zou, H. Dai, *Angew. Chem.* **2013**, 52, 13002.
- [22] M. Kamimura, S. Takahiro, M. Yoshida, Y. Hashimoto, R. Fukushima, K. Soga, *Polym. J.* **2017**, 49, 799.
- [23] S. J. Schambach, S. Bag, C. Groden, L. Schilling, M. A. Brockmann, *Methods* **2010**, 50, 26.
- [24] F. Kiessling, B. Pichler, P. Hauff, in *Small Animal Imaging*, Springer, New York **2017** pp. 155–161.
- [25] V. Ermolayev, X. L. Deán-Ben, S. Mandal, V. Ntziachristos, D. Razansky, *Eur. Radiol.* **2016**, 26, 1843.
- [26] A. Özbek, X. L. Deán-Ben, D. Razansky, *Optica* **2018**, 5, 857.
- [27] A. Ron, N. Davoudi, X. L. Deán-Ben, D. Razansky, *Appl. Sci.* **2019**, 9, 2737.
- [28] N. L. Ford, H. N. Nikolov, C. J. Norley, M. M. Thornton, P. J. Foster, M. Drangova, D. W. Holdsworth, *Med. Phys.* **2005**, 32, 2888.
- [29] S. J. Schambach, S. Bag, L. Schilling, C. Groden, M. A. Brockmann, *Methods* **2010**, 50, 2.
- [30] E. C. Dreaden, A. M. Alkilany, X. Huang, C. J. Murphy, M. A. El-Sayed, *Chem. Soc. Rev.* **2012**, 41, 2740.
- [31] K. Homan, S. Kim, Y. S. Chen, B. Wang, S. Mallidi, S. Emelianov, *Opt. Lett.* **2010**, 35, 2663.
- [32] C. Yin, G. Wen, C. Liu, B. Yang, S. Lin, J. Huang, P. Zhao, S. H. D. Wong, K. Zhang, X. Chen, *ACS Nano* **2018**, 12, 12201.
- [33] R. Su, S. A. Ermilov, A. Liopo, A. A. Oraevsky, *J. Biomed. Opt.* **2012**, 17, 101506.
- [34] J. Wang, Y. Xie, L. Wang, J. Tang, J. Li, D. Kocaefe, Y. Kocaefe, Z. Zhang, Y. Li, C. Chen, *RSC Adv.* **2015**, 5, 7529.
- [35] S. P. Egusquiaguirre, N. Beziere, J. L. Pedraz, R. M. Hernández, V. Ntziachristos, M. Igartua, *Contrast Media Mol. Imaging* **2015**, 10, 421.
- [36] R. Cheheltani, R. M. Ezzibdeh, P. Chhour, K. Pulaparthy, J. Kim, M. Jurcova, J. C. Hsu, C. Blundell, H. I. Litt, V. A. Ferrari, *Biomaterials* **2016**, 102, 87.
- [37] W. Song, Z. Tang, D. Zhang, N. Burton, W. Driessen, X. Chen, *RSC Adv.* **2015**, 5, 3807.
- [38] A. Ron, X. L. Deán-Ben, J. Reber, V. Ntziachristos, D. Razansky, *Mol. Imaging Biol.* **2019**, 21, 620.
- [39] Y.-S. Chen, Y. Zhao, S. J. Yoon, S. S. Gambhir, S. Emelianov, *Nat. Nanotechnol.* **2019**, 14, 465.
- [40] Y.-S. Chen, W. Frey, S. Kim, K. Homan, P. Kruizinga, K. Sokolov, S. Emelianov, *Opt. Express* **2010**, 18, 8867.
- [41] X. L. Deán-Ben, D. Razansky, *Opt. Express* **2013**, 21, 28062.
- [42] A. Rosenthal, V. Ntziachristos, D. Razansky, *Curr. Med. Imaging Rev.* **2013**, 9, 318.